Chapter 17
Simulation of Complex Networks

The concept of a *network* has been introduced in Chap. 2 as consisting of

- Branches, a branch being a contiguous series of components through which the working fluid flows,
- Nodes, being points of connection of branches with each other,
- Linking stubs, being points of connection to external interfacing components or atmosphere.

Each network is characterised by its working medium, which will usually, but not necessarily, be the same in each branch of the network, and by the treatment of the working fluid as incompressible or compressible. It is usual to treat fluids such as water, fuel and lubricating oils and slurries as incompressible for computation purposes. Low-pressure gas networks which work at pressures close to atmospheric can be treated as incompressible if they contain fans. If they contain compressors they are probably not operating close to a uniform pressure and should be treated as compressible. Steam and higher pressure gas networks should be treated as compressible, as should any branch involving phase change.

The issue of compressibility is not confined to questions of operating pressure range. Some low pressure gas systems are built using very large-diameter pipes extending over significant distances. Pressure changes in these pipes require the in- and outflows of considerable masses of gas. Examples of such systems are the blast furnace and coke oven gas networks around steelworks. Because of their large volumes and filling requirements, such networks should be treated as compressible even though their operating pressure ranges lie within the otherwise allowable incompressible range.

While it is almost always valid to treat the furnace air supply network, including forced draft, primary and seal air fans, hot and cold air ducts, dampers and air heater ducting, as incompressible, since treatment of the system dynamics adds little to simulation realism or accuracy, the same cannot be said of the flue gas system. With its large ducts and close dynamic interaction with the furnace, the flue gas system has a noticeable influence on longer-term furnace pressure variations.

P. O'Kelly, *Computer Simulation of Thermal Plant Operations*,
DOI 10.1007/978-1-4614-4256-1_17,

However, since acoustic wave effects associated with gas compressibility have been excluded from this treatment, the "organ-pipe" effects sometimes observed as a severe oscillation of furnace pressure following a rapid disturbance in the furnace or flue gas system cannot be reproduced by the modelling equations derived in this chapter.

The division of networks according to compressibility applies only to the method of calculation of the pressures and flows throughout the network. No distinction in made is the calculation of energy and temperature distributions although clearly, compression energy need not be considered for incompressible flows.

17.1 Incompressible Flow Networks

The assumption of incompressibility in each branch implies equal mass flow at every point between any given pair of nodes. Initially, branch flow inertia will be neglected ($\mathrm{d}\dot{m}/\mathrm{d}t = 0$) allowing the instantaneous flow to be determined from the branch lumped admittance and the differential pressure across the branch. The mass flow network can then be developed on the basis of continuity of mass at each node. Assume the network consists of n_{br} branches connecting internal nodes to each other, n_{bc} branches connecting internal nodes to external interfaces, and n_{nd} nodes.

Without assuming incompressibility of the fluid in the node[1], continuity at the jth node requires that

$$\sum_{i}^{n_{br}} \dot{m}_{ij} + \sum_{s}^{n_{bs}} \dot{m}_{sj} + \dot{m}_{ext} = \frac{\mathrm{d}M_j}{\mathrm{d}t} \tag{17.1}$$

where,

$\dot{m}_{ij}$ is the mass flow from node i to node j
$\dot{m}_{sj}$ is the mass flow from an external source s to node j
$\dot{m}_{ext}$ is a fixed flow (independent of node pressure) entering the node from an external source (−ve flow = outflow)
M_j is the mass of fluid in the jth node

Neglecting flow momentum, the mass flow through the ij-th branch connecting nodes i and j is given from

$$\dot{m}_{ij}^2 = \mathcal{A}_{ij}(p_i - p_j + g_{ij}) \tag{17.2}$$

[1]Had we assumed incompressibility of the fluid in the node, we would have been forced to set $\mathrm{d}\dot{m}_j/\mathrm{d}t = 0$ for each node. This would lead to an algebraic system for the solution of flows. This system can become singular for some perfectly normal equipment configurations and is therefore to be avoided. Alternatively, we could allow the volume of the node to vary, the sometimes called "rubber-hose" effect, and also to be avoided.

Similarly, the mass flow through the sj-th branch connecting the external source s and node j is given from,

$$\dot{m}_{sj}^2 = \mathcal{A}_{sj}(p_s - p_j + g_{sj}) \tag{17.3}$$

where,

$\mathcal{A}_{ij}$ is the branch admittance from node i to node j
$\mathcal{A}_{sj}$ is the branch admittance from source s to node j
g_{ij} is the combination of geodetic pressure height difference between nodes i and j plus any developed heads in the branch
g_{sj} is the same for the branch connecting source s to node j

With $M = \rho V$, the right-hand side of Eq. 17.1 can be expanded as,

$$\frac{\mathrm{d}M_j}{\mathrm{d}t} = V_j \frac{\partial \rho_j}{\partial p_j}\frac{\mathrm{d}p_j}{\mathrm{d}t} + V_j \frac{\partial \rho_j}{\partial T_j}\frac{\mathrm{d}T_j}{\mathrm{d}t}$$

Replacing $\mathrm{d}p_j/\mathrm{d}t$ by its discrete-time equivalent allows us to write

$$\frac{\mathrm{d}M_j}{\mathrm{d}t} = C_j\left(\frac{p_j^{n+1} - p_j^n}{\Delta t}\right) + \dot{m}_{th,j} \tag{17.4}$$

where $C_j = V_j \frac{\partial \rho_j}{\partial p_j}$ and is directly related to fluid compressibility ($\partial\rho/\partial p > 0$). The flow term $\dot{m}_{th,j}$ arises from the thermal expansion of the fluid and couples the mass and heat flow networks at the nodes.

Equation 17.2 can be linearised by noting that

$$\sqrt{\Delta p} = \frac{\Delta p}{\sqrt{|\Delta p|}} \text{ where } |\Delta p| > 0$$

Then,

$$\dot{m}_{ij} = A_{ij}(p_i - p_j + g_{ij}) \tag{17.5}$$

where

$$A_{ij} = \left[\frac{\mathcal{A}_{ij}}{(p_i - p_j + g_{ij})^n}\right]^{\frac{1}{2}} \tag{17.6}$$

The index n implies use of these quantities calculated at the previous time step.

Similarly for the source branches,

$$\dot{m}_{sj} = A_{sj}(p_s - p_j + g_{sj}) \tag{17.7}$$

where

$$A_{sj} = \left[\frac{\mathcal{A}_{sj}}{(p_s - p_j + g_{sj})^n}\right]^{\frac{1}{2}} \tag{17.8}$$

Combining Eqs. 17.1, 17.2, 17.5 and 17.7 and collecting like terms gives

$$-\frac{\Delta t}{C_j}\sum_i A_{ij}\,p_i^{n+1}+\left(1+\frac{\Delta t}{C_j}\sum_i A_{ij}+\frac{\Delta t}{C_j}\sum_s A_{sj}\right)p_j^{n+1}=p_j^n$$
$$+\frac{\Delta t}{C_j}\left(\sum_s A_{sj}\,p_s^n+\sum_i A_{ij}\,g_{ij}^n+\sum_s A_{sj}\,g_{sj}^n\right)-\frac{\Delta t}{C_j}\left(\dot{m}_{th,j}^n+\dot{m}_{ext}\right) \tag{17.9}$$

Equation 17.9 represents a set of n_{nd} equations in the node pressures p_j, given the external source pressures p_s and branch pressure heads g_{ij} and g_{sj} for each branch connecting to the jth node. The equation is written concisely in matrix form as

$$[\mathbf{I}+\mathbf{A_{dm}}]\,\mathbf{P^{n+1}}=\mathbf{P}^n+\frac{\Delta t}{C_j}\left[\mathbf{A_{bc}}\,\mathbf{P}_s+\mathbf{A_{dh}}\,\mathbf{G}-\mathbf{M_{th}}+\mathbf{M_{ext}}\right]$$
$$=\mathbf{P}^n+\frac{\Delta t}{C_j}\mathbf{S} \tag{17.10}$$

where each element on the RHS is evaluated at time n and

P	is a vector of node pressures at times $(n+1)$ and n
$\mathbf{P_s}$	is a vector of (external) source pressures
G	is a vector of net pressure heads in each branch
$\mathbf{M_{th}}$	is a vector of thermal expansion flows
$\mathbf{M_{ext}}$	is a vector of fixed external flows
$\mathbf{A_{dm}}$	is a matrix of admittances of branches connected to each internal node
$\mathbf{A_{bc}}$	is a matrix of admittances of branches connected to each external source
$\mathbf{A_{dh}}$	is a matrix of admittances of branches connecting to each node
I	is the unit matrix

The matrix $\mathbf{A_{dm}}$ is the network admittance matrix. The vector **S** is the network source vector.

Equation 17.10 is linear, and the admittance coefficient matrix is usually symmetric and positive-definite. Since all admittances have been linearised, solution of this equation is iterative, the iterations continuing until the node pressures have converged to within an acceptable tolerance. In practice very few iterations are required unless the system has been subjected to a large and sudden displacement from its previous state, and even then, convergence is rapid but transiently may exhibit noticeable dynamic errors. The individual branch flows are computed from Eq. 17.5 using the resulting node pressures.

Because the main diagonal elements are always ≥ 1 in magnitude (1 + some positive admittance which can be zero) the coefficient matrix $\mathbf{A_{dm}}$ will never be singular even if a specific node becomes totally isolated, that is, if the admittance of each branch joining the node is zero. For example, Eq. 17.10 will yield a stable solution for p_0 even if all three valves of Fig. 17.1 are closed.

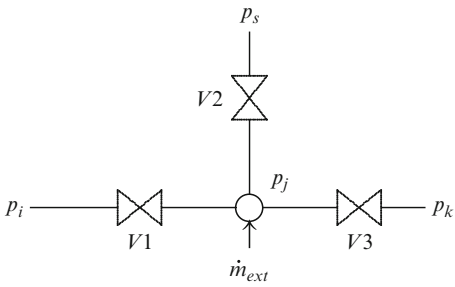

Fig. 17.1 Flow connections at a node

17.1.1 Inclusion of Flow Momentum

Because flow momentum has been neglected, in response to dynamically changing conditions, Eq. 17.10 generates a series of steady-state solutions to the network pressures and flows. In most cases, this is sufficient. However, as noted earlier, this can give rise to dynamic errors when things change rapidly. To avoid this, it is necessary to include flow inertia in the derivation of the node pressure and branch flow equations.

From Chap. 5 we have the original momentum conservation Eq. 5.11

$$\frac{\partial \phi}{\partial t} = -\left(1 + \phi^2 \frac{\partial v}{\partial p}\right) \frac{\partial p}{\partial z} - \phi^2 \frac{\partial v}{\partial h} \frac{\partial h}{\partial z} - 2\frac{\phi}{v} \frac{\partial v}{\partial t} - \left.\frac{\partial p}{\partial z}\right|_{loss} - \rho\, g\, \sin\beta$$

Restricting attention to the case $\phi^2 \frac{\partial v}{\partial p} \ll 1$ and neglecting the thermal expansion effects introduced by the term $\phi^2 \frac{\partial v}{\partial h} \frac{\partial h}{\partial z}$, this equation reduces to

$$\frac{\partial \phi}{\partial t} = -\frac{\partial p}{\partial z} - 2\frac{\phi}{v} \frac{\partial v}{\partial t} - \left.\frac{\partial p}{\partial z}\right|_{loss} - \rho\, g\, \sin\beta$$

or

$$\frac{\partial \phi}{\partial t} = -\frac{\partial p}{\partial z} - 2\frac{\phi}{v} \frac{\partial v}{\partial p} \frac{\partial p}{\partial t} - \left.\frac{\partial p}{\partial z}\right|_{loss} - \rho\, g\, \sin\beta$$

For incompressible flow $\frac{\partial v}{\partial p} = 0$. For compressible flow $\frac{\partial v}{\partial p} \approx -\frac{v}{p}$ and we have

$$\frac{\partial \phi}{\partial t} = -\frac{\partial p}{\partial z} + 2\frac{\phi}{p} \frac{\partial p}{\partial t} - \left.\frac{\partial p}{\partial z}\right|_{loss} - \rho\, g\, \sin\beta$$

We can assume for the present purpose that $\frac{\partial p}{\partial z} \gg 2\frac{\phi}{p} \frac{\partial p}{\partial t}$ which allows us to write

$$\frac{\partial \phi}{\partial t} = -\frac{\partial p}{\partial z} - \left.\frac{\partial p}{\partial z}\right|_{loss} - \rho\, g\, \sin\beta$$

Denoting the flow cross-sectional area by a_x, and replacing the spatial partial derivatives by the approximation $\frac{\Delta p}{\Delta z}$ we may write

$$\frac{1}{a_x}\frac{\mathrm{d}\dot{m}}{\mathrm{d}t} = -\frac{\Delta p}{\Delta z} - \left.\frac{\Delta p}{\Delta z}\right|_{loss} - \rho\, g\, \sin\beta$$

or

$$\frac{\Delta z}{a_x}\frac{\mathrm{d}\dot{m}}{\mathrm{d}t} = -\Delta p - \Delta p|_{loss} - \rho\, g\, \Delta z \sin\beta$$

Then, for a flow $\dot{m}_{ij}$ between two points i and j having pressures p_i and p_j

$$\begin{aligned} I_M \frac{\mathrm{d}\dot{m}_{ij}}{\mathrm{d}t} &= p_i - p_j + g_{ij} - \Delta p|_{loss} \\ &= \Delta p_{ij} - \Delta p|_{loss} \end{aligned} \tag{17.11}$$

where $g_{ij} = \rho\, g\, \Delta z \sin\beta$.

The coefficient $I_M = \Delta z/a_x$ is related to the parameter known as *inertance*[2]. Inertance is defined by the pressure gradient required to produce a given *volumetric* flow rate,

$$\Delta p = \rho \frac{\Delta z}{a_x}\frac{\mathrm{d}\dot{Q}}{\mathrm{d}t} = I\frac{\mathrm{d}\dot{Q}}{\mathrm{d}t}$$

with the inertance I given from

$$I = \rho\frac{\Delta z}{a_x}$$

It follows that

$$I_M = \frac{\Delta z}{a_x} = \frac{I}{\rho}$$

and is independent of the flow medium.

$\Delta p|_{loss}$ is the flow-dependent friction pressure loss across the branch, given by the standard equation

$$\mathcal{F}_{dp} = \Delta p|_{loss} = \frac{1}{\mathcal{A}_{ij}}\dot{m}_{ij}^2 \tag{17.12}$$

In Eq. 17.11 replace the continuous derivative by its discrete time equivalent to give

$$I_M\left(\frac{\dot{m}_{ij}^{n+1} - \dot{m}_{ij}^{n}}{dt}\right) = \Delta p_{ij}^{n+1} - \mathcal{F}_{dp} \tag{17.13}$$

[2]The term *inertance* is also found in the fields of acoustics and respiratory physiology.

Linearisation of the Friction Loss Term In an earlier section, linearisation of the friction pressure drop was handled by using the substitution

$$\sqrt{\Delta p^{n+1}} = \frac{\Delta p^{n+1}}{\sqrt{\Delta p^n}}$$

Here, we will use linearisation of $\mathcal{F}_{dp}$ by operating on $\dot{m}^2$ and consider two alternatives.

Version 1: $(\dot{m}^{n+1})^2 \approx \dot{m}^{n+1}\dot{m}^n$ Substituted into Eq. 17.13, this leads to

$$\dot{m}^{n+1} = \left(\frac{I_M \mathcal{A}_{ij}}{I_M \mathcal{A}_{ij} + \Delta t\, \dot{m}_{ij}^n}\right) \dot{m}_{ij}^n + \left(\frac{\Delta t \mathcal{A}_{ij}}{I_M \mathcal{A}_{ij} + \Delta t\, \dot{m}_{ij}^n}\right) \Delta p_{ij}^{n+1} \tag{17.14}$$

Version 2: Taylor Series Expansion Approximate $\mathcal{F}_{dp}$ by the first two terms of a Taylor series expansion about the known $\dot{m}_{ij}^n$.

$$\mathcal{F}_{dp}^{n+1} \approx \mathcal{F}_{dp}(\dot{m}_{ij}^n) + \left(\dot{m}_{ij}^{n+1} - \dot{m}_{ij}^n\right) \frac{\partial(\mathcal{F}_{dp})}{\partial \dot{m}_{ij}}.$$

With substitution of the derivative

$$\frac{\partial(\mathcal{F}_{dp})}{\partial \dot{m}_{ij}} = \frac{2}{\mathcal{A}_{ij}} \dot{m}_{ij}$$

this reduces to

$$\mathcal{F}_{dp}^{n+1} \approx \left(\frac{2}{\mathcal{A}_{ij}} \dot{m}_{ij}^n\right) \dot{m}_{ij}^{n+1} - \frac{1}{\mathcal{A}_{ij}} (\dot{m}_{ij}^n)^2$$

Again, substituted into Eq. 17.13 this leads to

$$\dot{m}_{ij}^{n+1} = \left(\frac{I_M\, \mathcal{A}_{ij} + \Delta t\, \dot{m}_{ij}^n}{I_M\, \mathcal{A}_{ij} + 2\Delta t\, \dot{m}_{ij}^n}\right) \dot{m}_{ij}^n + \left(\frac{\Delta t \mathcal{A}_{ij}}{I_M\, \mathcal{A}_{ij} + 2\Delta t\, \dot{m}_{ij}^n}\right) \Delta p_{ij}^{n+1} \tag{17.15}$$

By setting $\dot{m}_{ij}^{n+1} = \dot{m}_{ij}^n$, it can easily be shown that Eqs. 17.14 and 17.15 reduce to Eq. 17.2 in the steady state.

The bracketed coefficient terms in Eqs . 17.14 and 17.15 can be handled more simply by denominating them by ϑ and θ, respectively. Then, for Eq. 17.15,

$$\theta_{ij} = \frac{\Delta t \mathcal{A}_{ij}}{I_M\, \mathcal{A}_{ij} + 2\Delta t\, \dot{m}_{ij}^n} \tag{17.16}$$

and

$$\vartheta_{ij} = \frac{I_M\, \mathcal{A}_{ij} + \Delta t\, \dot{m}_{ij}^n}{I_M\, \mathcal{A}_{ij} + 2\Delta t\, \dot{m}_{ij}^n} \tag{17.17}$$

and an equivalent pair for Eq. 17.14.

For either form of linearisation, we can write

$$\dot{m}_{ij}^{n+1} = \vartheta_{ij}\, \dot{m}_{ij}^{n} + \theta_{ij}\, \Delta p_{ij}^{n+1} \tag{17.18}$$

Returning to Eq. 17.4, we have

$$p_j^{n+1} = p_j^n + \frac{\Delta t}{C_j} \sum_i \dot{m}_{ij} - \frac{\Delta t}{C_j}(\dot{m}_{th} - \dot{m}_{ex})$$

Summing $\dot{m}_{ij}$ from Eq. 17.18 over all branches connecting to the jth node, we can write

$$\sum_i \dot{m}_{ij}^{n+1} = \sum_i \vartheta_{ij}\, \dot{m}_{ij}^{n} + \sum_i \theta_{ij}\, p_i^{n+1} - \sum_i \theta_{ij}\, p_j^{n+1} + \sum_i \theta_{ij}\, g_{ij}^{n}$$

Combining this with Eq. 17.4, and separating terms dealing with internal branches from those dealing with branches to external sources to match the style of Eq. 17.10, we arrive at

$$\begin{aligned} &\frac{\Delta t}{C_j} \sum_i \theta_{ij}\, p_i^{n+1} + \left(1 + \frac{\Delta t}{C_j} \sum_i \theta_{ij} + + \frac{\Delta t}{C_j} \sum_s \theta_{sj}\right) p_j^{n+1} \\ &\quad = p_j^n + \frac{\Delta t}{C_j} \left(\sum_i \vartheta_{ij}\, \dot{m}_{ij}^n + \sum_s \theta_{sj}\, p_s^n + \sum_i \theta_{ij}\, g_{ij}^n + \sum_s \theta_{sj}\, g_{sj}^n\right) \\ &\qquad - \frac{\Delta t}{C_j} \left(\dot{m}_{th,j}^n + \dot{m}_{ex}\right) \end{aligned} \tag{17.19}$$

Taken over all nodes, Eq. 17.19 builds the equivalent of Eq. 17.10 but now includes the effects of flow inertia. Given the new node pressures and branch pressure differentials the new branch flows are computed from Eq. 17.18. All the coefficients of Eq. 17.19 can be computed using flows and admittances known from the previous time step.

Comparing with Eq. 17.10 we see that the two equations are identical in form. The introduction of flow momentum has added inertial terms to the calculation of the equation's coefficients. The other differences stem from the differing methods of admittance linearisation.

I_M appears as a factor multiplying $\mathcal{A}_{ij}$. Calling this product IA we can observe the following.

Equation 17.15 can be used to calculate a stable sequence for $\dot{m}^{n+1}$ if the coefficient of $\dot{m}^n$ is <1. This will always be the case though for $IA \gg 1$ this coefficient will approach 1 closely.

Conversely if $IA \ll 1$ then $\vartheta \approx \frac{1}{2}$ and $\theta \approx \frac{1}{2}\frac{\mathcal{A}_{ij}}{\dot{m}_{ij}^n}$. Then

$$\dot{m}_{ij}^{n+1} \approx 0.5\dot{m}_{ij}^n + 0.5\left(\frac{\mathcal{A}_{ij}}{\dot{m}_{ij}^n}\right)\Delta p_{ij}^{n+1} \tag{17.20}$$

For the first linearisation method, these results are valid for $IA \gg 1$. For $IA \ll 1$ however the effect of flow inertia disappears, and flow follows Δp with no or negligible delay.

For a pipe or duct section, admittance is proportional to a_x^2

$$\mathcal{A} = \frac{2\,d_h a_x^2}{\xi L\, v}$$

which, with $I_M = L/a_x$, gives for the product IA

$$IA = \frac{2\,d_h a_x}{\xi\, v}$$

17.1.2 Numerical Solution

In most cases, the topology of the physical system leads to the coefficient matrix of Eq. 17.10 being symmetric and positive definite. In this case the preferred solution method will be Cholesky decomposition. However, this situation cannot be guaranteed in every case and the best generic solution method, which will work virtually every time, is LU decomposition, preferably with pivoting.

17.2 Compressible Flow Networks

This section describes the derivation of a set of discrete-space equations for the computation of the time-varying pressures, flows, enthalpies and pressures within a complex network of branches carrying a compressible working medium. The starting point for these derivations is the set of conservation equations whose formulation in terms of one-dimensional discrete-space ordinate has been outlined in Sect. 5.3. The derivation applies generically to any arrangement of equipment within a branch. It follows from a consideration of the generic set of three cells shown by the following figure for a tube bank located within a gas duct transferring heat to a secondary fluid.

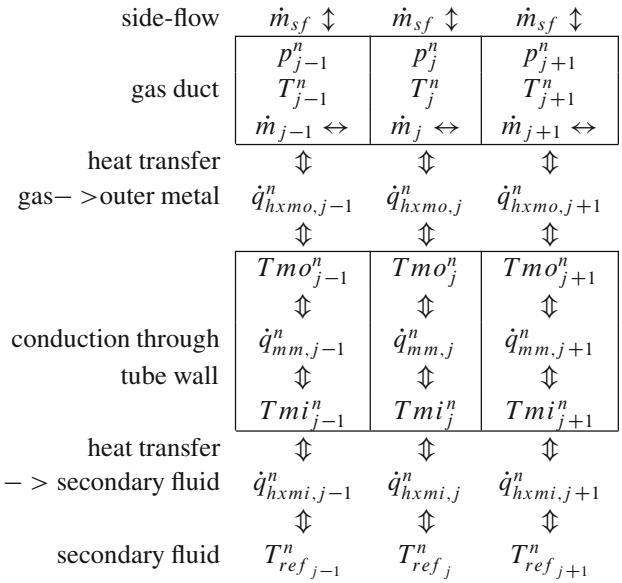

The symbols have the following meanings.

p	pressure in the jth spatial cell [kPa]
T	temperature in the jth spatial cell [°C]
h	specific enthalpy of the working fluid in the jth spatial cell [kJ/kg]
v	specific volume of the working fluid in the jth spatial cell [m^3/kg]
$\dot{m}_j$	mass flow between the $(j-1)$th and jth cells [kg/s]
$\dot{m}_{sf}$	side-flow mass in to or out of the cell, [kg/s]
h_{sf}	specific enthalpy of the side-flow into the jth cell [kJ/kg]
Tmi	temperature of wall inner zone metal in the jth spatial cell [°C]
Tmo	temperature of wall outer zone metal in the jth spatial cell [°C]
$\dot{q}_{hxmi}$	heat transfer between the primary working fluid and the wall in the jth spatial cell [kW]
$\dot{q}_{hxmo}$	heat transfer between the wall and the secondary working fluid in the jth spatial cell [kW]
$\dot{q}_{mm}$	heat transfer through the wall from the outer to the inner zones in the jth spatial cell [kW]
$Q = Mh$	total heat in the working fluid in the jth spatial cell [J]
M	total mass of working fluid in the jth cell [kg]
V	total volume of working fluid in the jth cell [m^3]
A_{hxmi}	heat transfer area on the inner surface of the jth cell wall [m^2]
A_{hxmo}	heat transfer area on the outer surface of the jth cell wall [m^2]
$A_{hxinsul}$	heat transfer area—lagging to ambient—on the outer surface of the jth cell lagging [m^2]
a_{xsect}	mass flow cross-section area per tube in jth cell [m^2]

T_{ref} is the reference temperature seen by $\dot{q}_{hxmi,j}$, either local ambient temperature for a pipe, pump, damper or ducting or secondary fluid temperature for a heat exchanger.

Two types of cell variables—cell centre and cell boundary variables—are defined [7]. Cell variables defined at cell centres are denoted by full indices. Cell variables defined at the boundaries are denoted by half-indices. Cell centre variables are determined from mass and energy balance equations which treat flows which cross the boundaries. Cell edge or boundary variables link the adjacent cells and are defined in terms of the adjacent cell centre variables.

17.2.1 The Conservation Equations: Flow Momentum Neglected

To avoid clutter, variables associated with the jth cell will in general not be indexed. Indexing of the jth cell variable will be used selectively to avoid ambiguities.

Mass Conservation From Eq. 5.36, Sect. 5.3.1, we have

$$\begin{aligned}\frac{\mathrm{d}M}{\mathrm{d}t} &= \sum(\dot{m})_j \\ &= \frac{\mathrm{d}}{\mathrm{d}t}\left(\frac{V}{v}\right) \\ &= -\frac{V}{v^2}\frac{\mathrm{d}v}{\mathrm{d}t}\end{aligned}$$

where

$$\sum(\dot{m})_j = \dot{m}_{j-1} - \dot{m}_j + \dot{m}_{sf}$$

Given that

$$v = f(p,h)$$

we may write

$$\frac{\mathrm{d}v}{\mathrm{d}t} = \frac{\partial v}{\partial p}\frac{\mathrm{d}p}{\mathrm{d}t} + \frac{\partial v}{\partial h}\frac{\mathrm{d}h}{\mathrm{d}t}$$

and

$$\frac{\partial v}{\partial p}\frac{\mathrm{d}p}{\mathrm{d}t} + \frac{\partial v}{\partial h}\frac{\mathrm{d}h}{\mathrm{d}t} = -\frac{v^2}{V}\sum(\dot{m})_j. \tag{17.21}$$

Equation 17.21 may be rearranged into

$$\frac{V}{v^2}\frac{\partial v}{\partial p}\frac{\mathrm{d}p}{\mathrm{d}t} + \frac{V}{v^2}\frac{\partial v}{\partial h}\frac{\mathrm{d}h}{\mathrm{d}t} = \dot{m}_{j-1} - \dot{m}_j + \dot{m}_{sf}. \tag{17.22}$$

Energy Conservation The energy balance for the jth cell may be written

$$\frac{\mathrm{d}(Mh)}{\mathrm{d}t} = \dot{m}_{j-1}h_{j-\frac{1}{2}} - \dot{m}_j h_{j+\frac{1}{2}} + \dot{m}_{sf}h_{sf} + V\frac{\mathrm{d}p}{\mathrm{d}t} - \dot{q}. \tag{17.23}$$

where the net heat flow $\dot{q}$ out of the cell is composed as $\dot{q} = \dot{q}_{hxm} + \dot{q}_{amb} - \dot{q}_{gen}$. $\dot{q}_{hxm}$ is the heat exchanged across the boundaries of the cell (+ve is conventionally out of the cell). $\dot{q}_{gen}$ is the heat generated within a cell by friction losses, chemical reactions, etc. $\dot{q}_{amb}$ is the heat transfer between the fluid and its surroundings. $h_{j-\frac{1}{2}}$ and $h_{j+\frac{1}{2}}$ are the enthalpies of the flows crossing the left and right hand boundaries of the jth cell respectively. Note that a positive $\dot{m}_{sf}$ is directed into the cell.

Expanding the left-hand side of Eq. 17.23 leads to

$$M\frac{\mathrm{d}h}{\mathrm{d}t} + h\frac{\mathrm{d}M}{\mathrm{d}t} = \dot{m}_{j-1}h_{j-\frac{1}{2}} - \dot{m}_j h_{j+\frac{1}{2}} + \dot{m}_{sf}h_{sf} + V\frac{\mathrm{d}p}{\mathrm{d}t} - \dot{q}$$

which, after substituting for $\frac{\mathrm{d}M}{\mathrm{d}t} = \sum(\dot{m})_j$, reduces to

$$M\frac{\mathrm{d}h}{\mathrm{d}t} = \dot{m}_{j-1}(h_{j-\frac{1}{2}} - h_j) - \dot{m}_j(h_{j+\frac{1}{2}} - h_j) + \dot{m}_{sf}(h_{sf} - h_j) + V\frac{\mathrm{d}p}{\mathrm{d}t} - \dot{q}. \tag{17.24}$$

The cell boundary enthalpies $h_{j-\frac{1}{2}}$ and $h_{j+\frac{1}{2}}$ may be expressed in terms of cell-centre enthalpies in the adjacent cells by defining,

$$h_{j-\frac{1}{2}} = \frac{(1+\varphi_{j-1})}{2}h_{j-1} + \frac{(1-\varphi_{j-1})}{2}h_j$$
$$h_{j+\frac{1}{2}} = \frac{(1+\varphi_j)}{2}h_j + \frac{(1-\varphi_j)}{2}h_{j+1},$$

where φ can take values in the range $(-1, +1)$ and reflects the direction of flow. The general form is,

$$\varphi_j = a \text{ if } \dot{m}_j > 0; \quad \varphi_j = -a \text{ if } \dot{m}_j < 0.$$

Full donor cell differences are obtained if $a = 1$. Selection of $a = 0$ results in the usual centre differencing.

The preceding equations may be rearranged as

$$\begin{aligned} h_{j-\frac{1}{2}} - h_j &= \tfrac{(1+\varphi_{j-1})}{2}(h_{j-1} - h_j) \\ h_j - h_{j+\frac{1}{2}} &= \tfrac{(1-\varphi_j)}{2}(h_j - h_{j+1}). \end{aligned} \tag{17.25}$$

With these substitutions and M replaced by V/v, Eq. 17.24 becomes

$$\begin{aligned} -V\frac{\mathrm{d}p}{\mathrm{d}t} + \frac{V}{v}\frac{\mathrm{d}h}{\mathrm{d}t} = {} & \frac{(1+\varphi_{j-1})}{2}\dot{m}_{j-1}(h_{j-1} - h_j) \\ & + \frac{(1-\varphi_j)}{2}\dot{m}_j(h_j - h_{j+1}) - \dot{q} + \dot{m}_{sf}(h_{sf} - h_j). \end{aligned} \tag{17.26}$$

The Coupled Mass and Energy Equations

The mass and energy conservation equations for the jth cell may be grouped into a single matrix equation. Writing

$$\begin{aligned} c_1 &= \frac{(1+\varphi_{j-1})}{2}(h_{j-1} - h_j), \\ c_2 &= \frac{(1-\varphi_j)}{2}(h_j - h_{j+1}), \\ c_3 &= h_{sf} - h_j. \end{aligned}$$

the composite equation can be written

$$\begin{bmatrix} \frac{V}{v^2}\frac{\partial v}{\partial p} & \frac{V}{v^2}\frac{\partial v}{\partial h} \\ -V & \frac{V}{v}. \end{bmatrix} \begin{bmatrix} \frac{\mathrm{d}p}{\mathrm{d}t} \\ \frac{\mathrm{d}h}{\mathrm{d}t} \end{bmatrix} = \begin{bmatrix} -1 & 1 \\ c_1 & c_2 \end{bmatrix} \begin{bmatrix} \dot{m}_{j-1} \\ \dot{m}_j \end{bmatrix} + \begin{bmatrix} -1 & 0 \\ c_3 & -1 \end{bmatrix} \begin{bmatrix} \dot{m}_{sf} \\ \dot{q} \end{bmatrix} \tag{17.27}$$

Inverting the left-hand side coefficient matrix and rearranging give

$$\begin{bmatrix} \frac{\mathrm{d}p}{\mathrm{d}t} \\ \frac{\mathrm{d}h}{\mathrm{d}t} \end{bmatrix} = \frac{1}{D}\begin{bmatrix} v & -\frac{\partial v}{\partial h} \\ v^2 & \frac{\partial v}{\partial p} \end{bmatrix} \begin{bmatrix} \text{right-hand side of Eq. 17.27} \end{bmatrix} \tag{17.28}$$

where,

$$D = V\left[\frac{1}{v}\frac{\partial v}{\partial p} + \frac{\partial v}{\partial h}\right]. \tag{17.29}$$

Since $\left|\frac{1}{v}\frac{\partial v}{\partial p}\right| > \frac{\partial v}{\partial h}$ and $\frac{\partial v}{\partial p}$ is always negative, so too is the determinant D.

The analytical solution of Eq. 5.19 of Sect. 5.2 revealed the high rate of decay of the pressure/flow transients compared to the rate of thermal effects. Subject to certain limitations which will be discussed later, we will initially ignore flow inertial effects and use the simplest form of the momentum equation:

$$\dot{m}_{j-1}^2 = \Omega_{j-1}\,(p_{j-1} - p_j + g_{j-1}),$$

where Ω_{j-1} is the flow admittance of the cell. Using the linearisation

$$\sqrt{\Delta p} = \frac{\Delta p}{\sqrt{\Delta p}}$$

and introducing the linearised cell admittance $\mathcal{A}$ we have

$$\dot{m}_{j-1} = \mathcal{A}_{j-1}\,(p_{j-1} - p_j + g_{j-1}),$$

where, for $|p_{j-1} - p_j + g_{j-1}| > 0$,

$$\mathcal{A}_{j-1} = \sqrt{\frac{\Omega_{j-1}}{|p_{j-1} - p_j + g_{j-1}|}}.$$

As used previously, g_j is the sum of developed and geodetic heads for the cell.

Any cell may be connected to a side-flow, either as an in- or outflow. The side flow $\dot{m}_{sf}$ to or from the jth cell is given from

$$\dot{m}_{sf} = \mathcal{A}_{sf}(p - p_{ref}),$$

where p_{ref} is the pressure at the other end of the side-flow path and $\mathcal{A}_{sf}$ is the admittance expressed in terms of an equivalent flow cross section,

$$\mathcal{A}_{sf} = \sqrt{\frac{\zeta\, A_{x,sf}^2}{|p - p_{ref}|}} \quad \text{for } |p - p_{ref}| > 0. \tag{17.30}$$

The expansion and reorganisation of Eq. 17.28 is facilitated by the following definitions:

$$\begin{aligned} a_1 &= v + \frac{\partial v}{\partial h}\frac{(1+\varphi_{j-1})}{2}(h_{j-1} - h_j),\\ a_2 &= v - \frac{\partial v}{\partial h}\frac{(1-\varphi_{j-1})}{2}(h_j - h_{j+1}),\\ a_3 &= v\frac{\partial v}{\partial h}(h_{sf} - h_j). \end{aligned} \tag{17.31}$$

and,

$$b_1 = \frac{\partial v}{\partial p}\frac{(1+\varphi_{j-1})}{2}\dot{m}_{j-1},$$
$$b_2 = \frac{\partial v}{\partial p}\left(-\frac{(1+\varphi_{j-1})}{2}\dot{m}_{j-1} + \frac{(1-\varphi_j)}{2}\dot{m}_j - \dot{m}_{sf}\right),$$
$$b_3 = -\frac{\partial v}{\partial p}\frac{(1-\varphi_j)}{2}\dot{m}_j. \tag{17.32}$$

from which it is apparent that,

$$b_2 = -b_1 - b_3 - \dot{m}_{sf}\frac{\partial v}{\partial p}.$$

The Decoupled Mass and Energy Equations

We can utilise the widely differing response rates of the underlying dynamics associated with pressure and enthalpy (or temperature) variations within the system to treat the mass and energy systems via separate but coupled pressure and enthalpy equations. Equation 17.28 may be expanded and separated into its two constituent equations as follows.

The Pressure Equation

$$\begin{aligned} D_j\frac{\mathrm{d}p_j}{\mathrm{d}t} = &-a_{1,j}\,\mathcal{A}_{j-1}\;p_{j-1} + [-a_{1,j}\,\mathcal{A}_{j-1} + a_{2,j}\,\mathcal{A}_j - a_{3,j}\,\mathcal{A}_{sf}]\,p_j \\ &- a_{2,j}\,\mathcal{A}_j\;p_{j+1} - a_{3,j}\,\mathcal{A}_{sf}\;p_{j,ref} + \frac{\partial v}{\partial h}\dot{q}_j \\ &+ a_{1,(j-1)}\mathcal{A}_{j-1}\mathrm{d}p_{j-1} - a_{1,j}\mathcal{A}_j\mathrm{d}p_j. \end{aligned} \tag{17.33}$$

The Enthalpy Equation

$$D_j\frac{\mathrm{d}h_j}{\mathrm{d}t} = -v_j^2 S(\dot{m}_j) + b_{1,j}h_{j-1} + b_{2,j}\,h_j + b_{3,j}\,h_{j+1} + \frac{\partial v}{\partial p}(\dot{m}_{sf}\,h_{sf} - \dot{q}_j), \tag{17.34}$$

where $S(\dot{m}_j) = \dot{m}_{j-1} - \dot{m}_j$

17.2.2 Solution of the Branch Equations

The first step is to reorganise Eqs. 17.33 and 17.34 into discrete-time form by replacing the continuous derivatives by their first-order discrete-time approximations. The original equations are then rearranged into implicit form.

The following coefficients are defined.

$$
\begin{aligned}
B_{j,j-1} &= -\frac{\Delta t}{D}\, a_1\, \mathcal{A}_{j-1} \\
B_{j,j+1} &= \frac{\Delta t}{D} a_2\, \mathcal{A}_j \\
B_{j,j} &= 1 - B_{j,j-1} - B_{j,j+1} \\
C_{j,j-1} &= -\frac{\Delta t}{D} b_1 \\
C_{j,j+1} &= -\frac{\Delta t}{D} b_3 \\
C_{j,j} &= 1 + \frac{\Delta t}{D} b_2 \\
Y_j &= \frac{\Delta t}{D}\left[v\, S(\dot{m}) + a_3 \dot{m}_{sf} - \frac{\partial v}{\partial h}\left((\dot{m}h)_{in} - \dot{m}_{cd}\, h'' - \dot{q} \right) \right] \\
Z_j &= \frac{\Delta t}{D}\left[v^2 S(\dot{m}_j) + \frac{\partial v}{\partial p}\left((\dot{m}h)_{in} - \dot{m}_{cd}\, h'' - \dot{q} \right) \right]
\end{aligned}
$$

The condensation term $\dot{m}_{cd}\, h''$ applies only to a condensing working medium such as steam, for which phase changes must be considered.

The pressure and enthalpy equations may then be written compactly as,

$$B_{j,j-1}\, p_{j-1}^{n+1} + B_{j,j}\, p_j^{n+1} + B_{j,j+1}\, p_{j+1}^{n+1} = p_j^n + Y_j . \tag{17.35}$$

$$C_{j,j-1}\, h_{j-1}^{n+1} + C_{j,j}\, h_j^{n+1} + C_{j,j+1}\, h_{j+1}^{n+1} = h_j^n + Z_j . \tag{17.36}$$

Equations 17.35 and 17.36 form a coupled set of mass and energy balance equations. The coefficients of each depend on the solution of the other through the coefficients a_1, a_2, b_1, etc., and the equation pair must be solved iteratively.

As j is taken over all n_{cell} contiguous cells in a branch, the pressure and enthalpy equations form two tridiagonal matrix equations. Boundary conditions are required at each end ($j = 1$ and $j = n_{cell}$). These are provided by the appropriate state variables of the interconnecting components.

When written out for all j for, say, a 7-cell section, Eqs. 17.35 and 17.36 form a tridiagonal matrix (the enthalpy equation is shown as the example).

$$\begin{bmatrix} C_{1,1} & C_{1,2} & & & & & \\ C_{2,1} & C_{2,2} & C_{2,3} & & & & \\ & C_{3,2} & C_{3,3} & C_{3,4} & & & \\ & & C_{4,3} & C_{4,4} & C_{4,5} & & \\ & & & C_{5,4} & C_{5,5} & C_{5,6} & \\ & & & & C_{6,5} & C_{6,6} & C_{6,7} \\ & & & & & C_{7,6} & C_{7,7} \end{bmatrix} \begin{bmatrix} h_1 \\ h_2 \\ h_3 \\ h_4 \\ h_5 \\ h_6 \\ h_7 \end{bmatrix}^{n+1}$$

$$= \begin{bmatrix} h_1 \\ h_2 \\ h_3 \\ h_4 \\ h_5 \\ h_6 \\ h_7 \end{bmatrix}^{n} + \begin{bmatrix} C_{1,0}h_0 \\ 0 \\ 0 \\ 0 \\ 0 \\ 0 \\ C_{7,8}h_8 \end{bmatrix}^{n} + \begin{bmatrix} Z_1 \\ Z_2 \\ Z_3 \\ Z_4 \\ Z_5 \\ Z_6 \\ Z_7 \end{bmatrix}^{n}. \tag{17.37}$$

where h_0 and h_8 are boundary conditions and are the enthalpies either in interfacing components or in internal nodes of the network.

Solution of this equation yields the map of working fluid enthalpies for each of the branch cells.

A similar matrix equation is constructed for pressures, with the C coefficients replaced by B coefficients, the Z vector replaced by the Y vector and with pressure boundary conditions defined in place of enthalpy boundary conditions.

Inclusion of Thermal Diffusion

The form of the advection equation makes no provision for the transfer of thermal energy between cells in the absence of flow. Once flow ceases in a cell or branch, enthalpy changes depend only on heat exchange across the boundaries with ambient or interfacing systems. These exchanges are very small and the attendant changes in enthalpy and temperature are correspondingly small and slow. Plant operations frequently result in the isolation of branches through which the working medium had previously been flowing. The medium within these isolated branches will cool, both by this slow ambient heat loss and by diffusion of energy throughout the stationary working medium. The ambient heat loss is included in the foregoing treatment but the diffusion influence is not. For this purpose, we must add a diffusion term to the original energy equation. Equation 17.23 then becomes

$$\frac{\mathrm{d}(Mh)}{\mathrm{d}t} = \dot{m}_{j-1}h_{j-\frac{1}{2}} - \dot{m}_j h_{j+\frac{1}{2}} + \dot{m}_{sf}h_{sf} + V\frac{\mathrm{d}p}{\mathrm{d}t} - \dot{q} + c_{dif}\frac{\partial^2 h}{\partial z^2}. \tag{17.38}$$

Using the spatial discretisation

$$\frac{\partial^2 h_j}{\partial z^2} = \frac{h_{j-1} - 2h_j + h_{j+1}}{\Delta z^2}$$

diffusion may be included by the modification of the C-coefficients as follows.

$$C_{j,j-1} = -\frac{\Delta t}{D}(b_1 - c_{dif}/\Delta z^2),$$
$$C_{j,j+1} = -\frac{\Delta t}{D}(b_3 - c_{dif}/\Delta z^2),$$
$$C_{j,j} = 1 + \frac{\Delta t}{D}(b_2 - 2c_{dif}/\Delta z^2).$$

where Δz is the length of the cell. The diffusion coefficient c_{dif} is given from Eq. 10.1

$$c_{dif} = \frac{\lambda}{c_p \rho}.$$

λ is the coefficient of thermal conductivity of the material, ρ is its density and c_p the specific heat capacity. For water, c_{dif} is typically around 1.5e-7. For saturated steam at 10 bar, c_{dif} = 2.76e-6 and at 160 bar, 1.45e-7. For superheated steam it lies in the range of 1e-6 to 5e-7. Since the observable effects of diffusion are slow and noticeable only during cooldown, a phase marked by very low or zero mass flows as temperatures tend towards those of their surroundings, the choice of a value for c_{dif} around 1.0e-7 is not critical.

Treatment of Boundary Conditions

Each branch has a left-and a right-hand end. Conventionally, the flow into the left-hand end and leaving the right-hand end cell is positive. A branch connects at each end to either an internal network node or an external device. Denoting by the index -1 the pressure or flow enthalpy at the left-hand end and by $+1$ that at the right-hand interface, we can write for the left-hand end

$$p_0^{n+1}\left(1 + \frac{\Delta t}{D_0}\mathcal{A}_0\right) - \frac{\Delta t}{D_0}\mathcal{A}_0 p_1^{n+1} = p_0^n + \frac{\Delta t}{D_0}\dot{m}_{-1}$$
$$= p_0^n + \frac{\Delta t}{D_0}\mathcal{A}_{-1}(p_{-1} - p_0)$$

and for the right hand end (Nth cell)

$$p_N^{n+1}\left(1+\frac{\Delta t}{D_N}\mathcal{A}_N\right)-\frac{\Delta t}{D_N}\mathcal{A}_N\,p_{N-1}^{n+1}=p_N^n+\frac{\Delta t}{D_N}\dot{m}_{+1}$$
$$=p_N^n+\frac{\Delta t}{D_N}\mathcal{A}_{+1}(p_N-p_{+1}).$$

17.2.3 Network of Multiple Branches

Equation 17.37 defines the map of steam enthalpies for a set of n_{cell} cells in a single branch. A network consists of n_{br} branches. The coefficient matrix of the composite equation for the entire network is composed of a set of coefficient submatrices, each of the form of Eq. 17.37. The network enthalpy state vector is composed of a set of subvectors, one for each branch and of dimension equal to the number of cells in the respective branch. The composite network equation is then of the form

$$\begin{bmatrix} C_1 & & & & \\ & C_2 & & & \\ & & \ddots & & \\ & & & C_{ibr} & \\ & & & & \ddots \\ & & & & & C_{nbr} \end{bmatrix} \begin{bmatrix} \vec{h}_1 \\ \vec{h}_2 \\ \vdots \\ \vec{h}_{ibr} \\ \vdots \\ \vec{h}_{nbr} \end{bmatrix}^{n+1}$$
$$= \begin{bmatrix} \vec{h}_1 \\ \vec{h}_2 \\ \vdots \\ \vec{h}_{ibr} \\ \vdots \\ \vec{h}_{nbr} \end{bmatrix}^{n} + \begin{bmatrix} h\vec{b}c_1 \\ h\vec{b}c_2 \\ \vdots \\ h\vec{b}c_{ibr} \\ \vdots \\ h\vec{b}c_{nbr} \end{bmatrix}^{n} + \begin{bmatrix} \vec{Z}_1 \\ \vec{Z}_2 \\ \vdots \\ \vec{Z}_{ibr} \\ \vdots \\ \vec{Z}_{nbr} \end{bmatrix}^{n} . \tag{17.39}$$

The presence of the $\vec{}$ above a symbol denotes a complete subvector for a single branch. $h\vec{bc}_{ibr}$ denotes a vector of boundary conditions for the (ibr)th branch. This vector will have non-zero entries in only the first and last elements.

At the points (nodes) at which branches join, boundary conditions are defined by the node enthalpies and pressures. Boundary enthalpies are required only for points of inflow to the branch and are selected for each branch on the basis of branch entry flow direction.

17.2.4 Calculation of Node Pressures

Node pressures may be included either explicitly as boundary conditions to the network branches or implicitly as elements of the network pressure vector.

The node pressures $\bar{p}_k$ are adjusted to ensure that the net mass flow at the kth node is balanced at each time step. The net flow balance will be exact for incompressible flow. For compressible nodes transient imbalances of inlet and outlet flows will reflect the mass changes within the node volumes. Denoting by M the mass of working medium in the kth node, conservation of mass requires

$$\frac{\mathrm{d}M}{\mathrm{d}t} = \sum_i \mathcal{A}_i (p_i - \bar{p}_k) + \Sigma(\dot{m}_{ext}), \tag{17.40}$$

where $\mathcal{A}_i$ is the (linearised) admittance of the flow cell linking the ith cell and kth node and p_i is the pressure in the ith cell adjacent to the kth node. This will be either the first cell if the left-hand branch end connects to the node or the last cell if the right-hand end connects. $\Sigma(\dot{m}_{ext})$ is the sum of flows entering or leaving the node to external branches or systems. With V_k the volume of the kth node, $M = V_k/v_k$, giving

$$\begin{aligned}
\frac{\mathrm{d}M}{\mathrm{d}t} &= \frac{\mathrm{d}}{\mathrm{d}t}\left(\frac{V_k}{v_k}\right) \\
&= -\left(\frac{V_k}{v_k^2}\right)\frac{\mathrm{d}v_k}{\mathrm{d}t} \\
&= -\left(\frac{V_k}{v_k^2}\right)\frac{\partial v}{\partial p}\frac{\mathrm{d}\bar{p}_k}{\mathrm{d}t} \\
&= \left(\frac{V_k}{\gamma\,\bar{p}_k v_k}\right)\frac{\mathrm{d}\bar{p}_k}{\mathrm{d}t}.
\end{aligned}$$

External Treatment of Node Pressures

With this substitution for $\mathrm{d}M/\mathrm{d}t$ and replacement of $\mathrm{d}\bar{p}_k/\mathrm{d}t$ by its discrete time equivalent, Eq. 17.40 can be expressed in implicit form, giving for $\bar{p}_k^{n+1}$

$$\bar{p}_k^{n+1} = \frac{\left[\bar{p}_k^n + \frac{\Delta t}{\tau_k}\left(\sum_i \mathcal{A}_i\; p_i^n + \Sigma(\dot{m}_{ext})\right)\right]}{\left[1 + \frac{\Delta t}{\tau_k}\sum_i \mathcal{A}_i\right]}, \tag{17.41}$$

where

$$\tau_k = \frac{V_k}{\gamma\,\bar{p}_k\,v_k} = \frac{V_k}{\gamma R \mathcal{T}_k}. \tag{17.42}$$

Internal Treatment of Node Pressures

A composite network pressure vector $\mathbf{P}$ is formed by augmenting the cell pressure vector $\mathbf{p}$ by the vector of node pressures $\bar{\mathbf{p}}$

$$\mathbf{P} = [\mathbf{p}\ \bar{\mathbf{p}}]^T.$$

For a boundary cell, Eq. 17.35 expresses the jth cell pressure in terms of its adjacent upstream cell $(j-1)$ and its connecting boundary pressure $\bar{p}_k$.

$$B_{j,j-1}\, p_{j-1}^{n+1} + B_{j,j}\, p_j^{n+1} + B_{j,j+1}\, \bar{p}_k^{n+1} = p_j^n + Y_j$$

or, expanding the B coefficients,

$$-\frac{\Delta t}{D_j} a_1 \mathcal{A}_{j-1} p_{j-1}^{n+1} + \left(1 + \frac{\Delta t}{D_j} a_1 \mathcal{A}_{j-1} + \frac{\Delta t}{D_j} a_2 \mathcal{A}_j\right) p_j^{n+1} + \frac{\Delta t}{D_j} a_2 \mathcal{A}_j\, \bar{p}_k^{n+1} = p_j^n + Y_j. \tag{17.43}$$

With some minor simplifications

$$D = V\left[\frac{1}{v}\frac{\partial v}{\partial p} + \frac{\partial v}{\partial h}\right] \approx \frac{V}{v}\frac{\partial v}{\partial p} \approx -\frac{V}{v}\frac{v}{p} = -\frac{V}{p}.$$

Therefore, given $p\, v = R\mathcal{T}$,

$$-\frac{\Delta t}{D_j} a_1 = -\Delta t \frac{R\mathcal{T}_j}{V_j}.$$

Similarly

$$\frac{\Delta t}{D_j} a_2 = -\Delta t \frac{R\mathcal{T}_j}{V_j}$$

and the cell equation becomes

$$-B_{j,j-1} p_{j-1}^{n+1} + (1 + B_{j,j-1} + B_{j,k}) p_j^{n+1} - B_{j,k}\, \bar{p}_k^{n+1} = p_j^n + Y_j^n, \tag{17.44}$$

where

$$B_{j,j-1} = \Delta t \frac{R\mathcal{T}_j}{V_j} \mathcal{A}_{j-1}.$$

$$B_{j,k} = \Delta t \frac{R\mathcal{T}_j}{V_j} \mathcal{A}_j.$$

For the kth node, the mass balance Eq. 17.40 can be rearranged into

$$\left(1 + \frac{\Delta t}{\tau_k}\sum_i \mathcal{A}_k\right)\bar{p}_k - \frac{\Delta t}{\tau_k}\sum \mathcal{A}_i\, p_i = \bar{p}_k^n + \frac{\Delta t}{\tau_k}\Sigma(\dot{m}_{ext}). \tag{17.45}$$

The augmented network equation can then be written

$$\begin{bmatrix}\mathbf{B}_{11} & \mathbf{B}_{12}\\ \mathbf{B}_{21} & \mathbf{B}_{22}\end{bmatrix}\begin{bmatrix}\mathbf{p}\\ \bar{\mathbf{p}}\end{bmatrix}^{n+1} = \begin{bmatrix}\mathbf{p}\\ \bar{\mathbf{p}}\end{bmatrix}^{n} + \begin{bmatrix}\mathbf{Y}\\ 0\end{bmatrix} + \begin{bmatrix}\mathbf{p}_{\text{bc}}\\ \frac{\Delta t}{\tau_k}\sum(\dot{m})\end{bmatrix}, \tag{17.46}$$

where the elements of the submatrices $\mathbf{B}_{11}$, $\mathbf{B}_{12}$, $\mathbf{B}_{21}$ and $\mathbf{B}_{22}$ are given from Eqs. 17.44 and 17.45.

Equation 17.46 is nearly tridiagonal. $\mathbf{B}_{11}$ is purely tridiagonal and $\mathbf{B}_{22}$ is purely diagonal. $\mathbf{B}_{12}$ and $\mathbf{B}_{21}$ contain the terms linking the branch end cells to their interfacing nodes and, in general, are sparse. The solution method described in Sect. 3.7.5 can be applied here.

It turns out that, not only is it not necessary to solve the augmented equation, it is advantageous to un-bundle the single augmented equation into two separate equations, one for the branch cell pressures $\mathbf{p}$ and one for the node pressures $\bar{\mathbf{p}}$, and solve them sequentially. The procedure then becomes
Solve:

$$\mathbf{B}_{11}\,\mathbf{p}^{n+1} = \mathbf{p}^n + \mathbf{Y} + \mathbf{p}_{\text{bc}} \tag{17.47}$$

for $\mathbf{p}^{n+1}$. Then

Calculate $\bar{\mathbf{p}}^{n+1}$ from:

$$\bar{\mathbf{p}}^{n+1} = \mathbf{B}_{22}^{-1}\left[\bar{\mathbf{p}}^n - \mathbf{B}_{21}\mathbf{p}^{n+1} + \frac{\Delta t}{\tau_k}\sum(\dot{m})\right]. \tag{17.48}$$

The advantage of the unbundled approach over the augmented is computation speed—the un-bundled approach is much faster—and numerical stability. Both Eqs. 17.47 and 17.48 are absolutely stable and allow the use of actual physical dimensions in the calculation of the equation coefficients. As a result they converge rapidly and stably. The off-diagonal elements of Eq. 17.46 introduce stability issues and their magnitude must be limited to less than the main diagonal elements to preserve diagonal dominance.

17.2.5 Calculation of Node Enthalpies and Temperatures

For incompressible flow, enthalpies at a mixing point depend only on the incoming stream enthalpies and on the time taken for the streams to mix homogeneously. These mixing times will be extremely short, particularly for high flow rates and small mixing volumes. At very low flow rates, mixing times could be longer, but enthalpy changes are unlikely to be large.

For the jth network node,

$$\tau_j \frac{\mathrm{d}h_j}{\mathrm{d}t} = \sum_i \dot{m}_i h_i - h_j \sum_i \dot{m}_i$$
$$= \sum_i \dot{m}_i (h_i - h_j),$$

where τ is the assumed mixing time constant [seconds], $\dot{m}_i$ is the mass flow from the ith branch into the jth node, h_i is the enthalpy of the flow leaving the jth branch and h_j is the medium enthalpy at the jth node.

Replacing the derivative by its discrete-time equivalent, we may write

$$h_j^{n+1} = h_j^n + \frac{\Delta t}{\tau_j} \sum_i \dot{m}_i (h_i - h_j)$$

which is written in fully implicit form as

$$h_j^{n+1} = \frac{[h_j^n + \frac{\Delta t}{\tau_j} \sum_i \dot{m}_i h_i^n]}{[1 + \frac{\Delta t}{\tau_j} \sum_i \dot{m}_i]}. \tag{17.49}$$

For a flow leaving a branch in the positive sense, h_i is the medium enthalpy in the last branch cell. For a flow leaving a branch in the negative sense, h_i is the medium enthalpy in the first branch cell.

17.2.6 Wall Temperature Calculation

The working medium, incompressible or compressible, flowing through the network is contained by the walls of a variety of components including pipes, valves, ducts, dampers, heat exchangers and so on that make up the physical network. These exchange heat with the medium—in the case of heat exchangers, with media on both sides of the wall—and with their surroundings, frequently through an insulating layer. The heat flows thus exchanged are represented in the preceding equations as $\dot{q}_{hxm}$, calculated for each cell from the local medium-wall temperature differential, assuming normal convective heat transfer. This means that the wall metal temperatures must be calculated simultaneously with the working fluid temperatures for each cell in the network.

The calculation method and arrangement of wall temperatures described in Sect. 10.3 is suitable for this purpose and can be linked directly with the network cell structure described above. The result is an integrated procedure that yields, within the scope of a single calculation, a complete map of the pressures, flows,

enthalpies, temperatures and derived properties for the working medium, together with two wall metal temperatures, for each cell and node of the complete network.

17.2.7 Application to a Typical Steam Flow Network

The methods of the preceding sections are illustrated by an example based on a real steam flow and heat exchange network. The following schematic depicts the parallel steam paths from a drum or water separators to the HP turbine of a power-generating unit. All branches are treated as compressible.

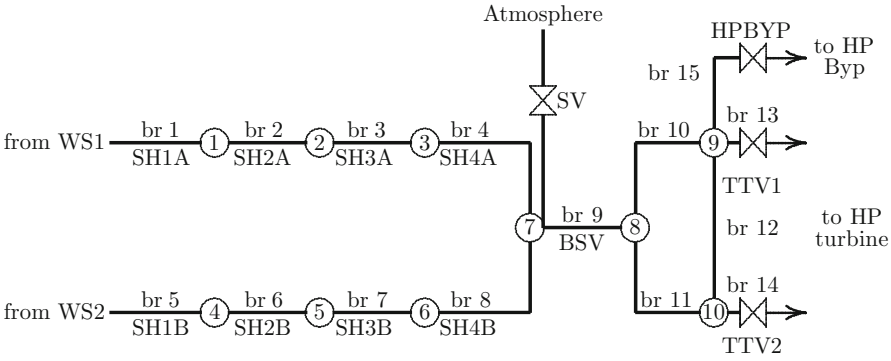

Branches 1–8 contain superheaters connected by pipes and headers. Superheaters are treated as tubular heat exchangers with a tube side (steam) and a duct or gas side. Each superheater is represented by a series of five contiguous cells. Connecting pipes contain between one and three cells, depending on length, are 250–300 mm NB, with a wall thickness of 7 mm and between 5 and 35 m long. Nodes 1–6 represent spray desuperheaters. Node 7 is the boiler outlet header which connects to node 8 via a short branch which includes the boiler stop valve (BSV). A safety valve (SV) to atmosphere is connected to node 7. Branches 10 and 11 are the long steam pipes (55 m, 9 cells) which terminate at the HP turbine stop/throttle valves. The two valve chests are connected by a short crossover pipe (branch 12). Steam flows to the HP turbine from nodes 9 and 10 through each of two throttle valves TTV1 and TTV2 are adjusted by modulating the valve positions to follow a preset loading program. In this exercise the turbine itself is not simulated. For the purpose of the demonstration, boundary conditions are defined by preset ramps of pressures as might be followed during a typical start of a generating unit but without the long holding periods normally used for turbine warming.

The associated (simplified) gas flow network is shown by the following figure.

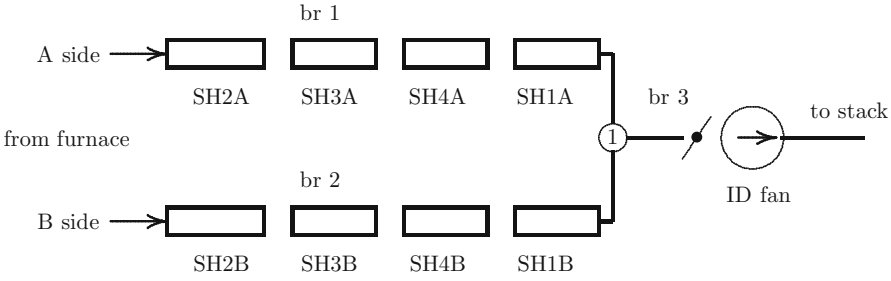

Obvious simplifications include omission of reheaters, economiser and airheater(s) from the gas flow paths and use of a single induced draft fan. One or more reheater tube banks might be interleaved with the superheater banks ahead of the primary superheater. It is to be noted that, following normal plant design, the primary superheaters SH1A/B are placed first in the steam flow path (lowest steam temperatures) and last in the gas flow path (lowest gas temperatures) and are connected in a counter-flow arrangement.

Network Behaviour: Flow Momentum Ignored

The calculation covers the following scope of operations which might form part of a unit start. Variations of pressures, flows and temperatures are shown. Following a typical start procedure, boiler steam pressure was initially increased to around 3,100 kPa (30 bar) using only igniters, giving a furnace exit gas temperature of around 450°C. With the boiler stop valve open, steam flows into the main steam system remained small, being only steam used to fill and pressurise the piping and superheater tubing and to make up steam lost as condensate through the boiler and steam line drains and vents. Steam pressure at the turbine stop valves was held at 3,100 kPa (30 bar) (A)[3] by modulating the position of the HP bypass valve, connected to node 9. During this time, the turbine might be accelerated to some intermediate speed, typically 1,000 rpm (for a 50 Hz system), and held there for initial warming while steam flows through the system increased to equal that passing through the bypass plus any losses through drain valves and vents. After a wait period of some 15 minutes, the pressure was increased to around 6,100 kPa (60 bar) by increasing the HP bypass valve pressure setpoint. The bypass valve closed (B) and steam flows reduced to their previous small values. Once the stop valve pressure reached its target the bypass valve again opened (C) to regulate pressure. Along the way, the first coal pulverisers would have been started, producing a rapid rise of furnace exit temperature to around, say, 650°C. The turbine would now be accelerated to synchronous speed. After synchronising to the grid (D) and initial loading (E), pressure was raised uniformly to the normal operating pressure of

[3]These letters refer to the those used on the trend graphs to identify points in the procedure.

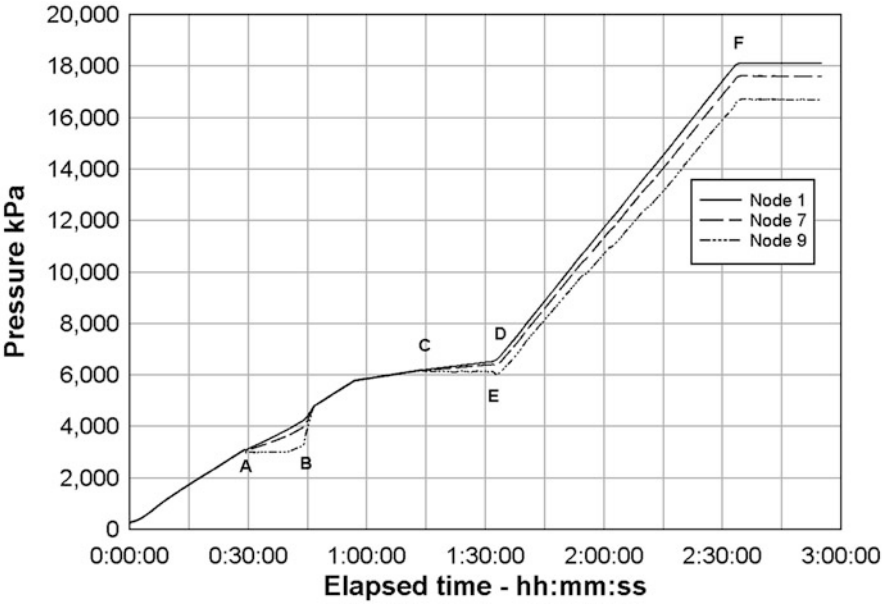

Fig. 17.2 Network pressure trends

18,700 kPa (185 bar) (F) at 2 bar/min while loading the turbine to 100 %. Additional pulverisers will have been started to match the increasing firing with increasing unit load. Each pulveriser start brought a rapid increase in furnace exit temperature which continued to increase with increased firing up to around 60 % load, after which it remains relatively constant at (here) 1,050°C. Full-load steam flow to the turbine was 330 kg/s and flue gas flow 300 kg/s (Figs. 17.2 and 17.3).

The increasing spread among the individual pressure trends indicates the increasing pressure drops through the system with increasing steam flows.

Figure 17.4 shows trends of individual steam temperatures. In the generation of these results, a very simplified method was used to match firing rate, and with it furnace exit temperature, to steam demand. As a consequence, the gas temperature entering the superheater duct changes in a somewhat unrealistic manner. The trends shown by Fig. 17.4 are not to be taken as representative of real plant behaviour. They do however allow realistic interpretation, given the other parameters of the simulated start. For example, during periods of low steam flow through the tubes, the superheater tube metal and steam temperatures rise quickly, possibly into alarm ranges, before reducing quickly once the steam flow increases as the bypass valve opens. The increase in steam temperatures during loading is typical (though excessive) and reflects the higher heat input into the steam as both firing rate and in particular the radiant contribution to the secondary and tertiary superheaters increase more rapidly than the steam flow through them. In practice, it would be expected that the steam temperature control desuperheating sprays (not included here) would

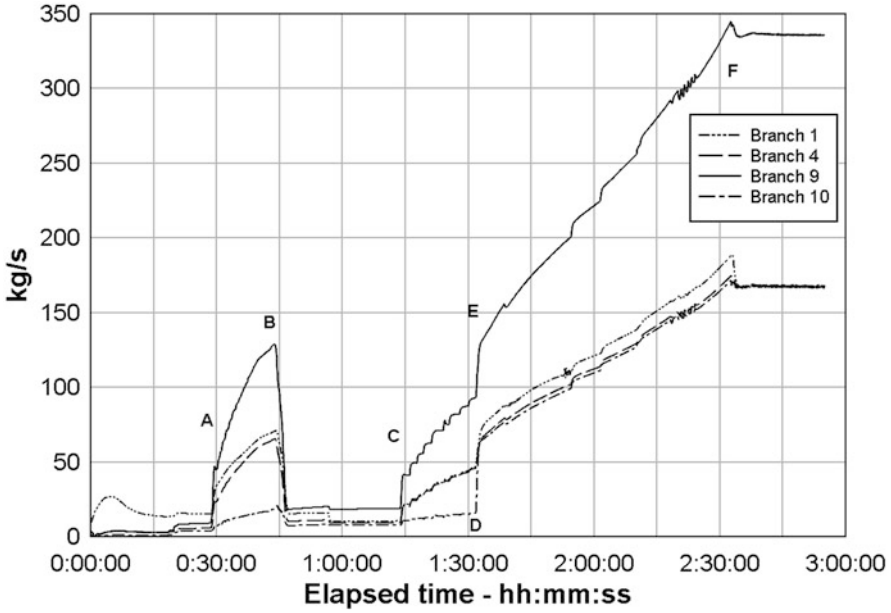

Fig. 17.3 Network flow trends

intervene to maintain set point values. As the steam flow increased beyond some 80 % of full load, the steam temperatures reduced to their normal operating values.

An allowance has been made in these calculations for the radiant heat contributions to the secondary and tertiary superheaters. Without this contribution, convective heat transfer alone would yield a lower boiler outlet temperature for this arrangement of superheaters and gas temperatures, as shown by the following simple calculation.

On the gas side,

Furnace exit temperature is set to 1,050°C
Flue gas temperature to the economiser is 415°C
Flue gas flow is 300kg/s
Flue gas mean specific heat is around 1.25 kJ/kg/C

Convective heat transfer gas side is

$$300 \times 1.25 \times (1{,}050 - 415) = 238{,}080\,\text{kJ/s}.$$

On the steam side,

Boiler steam pressure is 18,700 kPa
Boiler drum steam temperature = saturation temperature is then 359°C
Boiler drum saturation specific enthalpy is 2,493.8 kJ/kg
Total steam flow is 330 kg/s

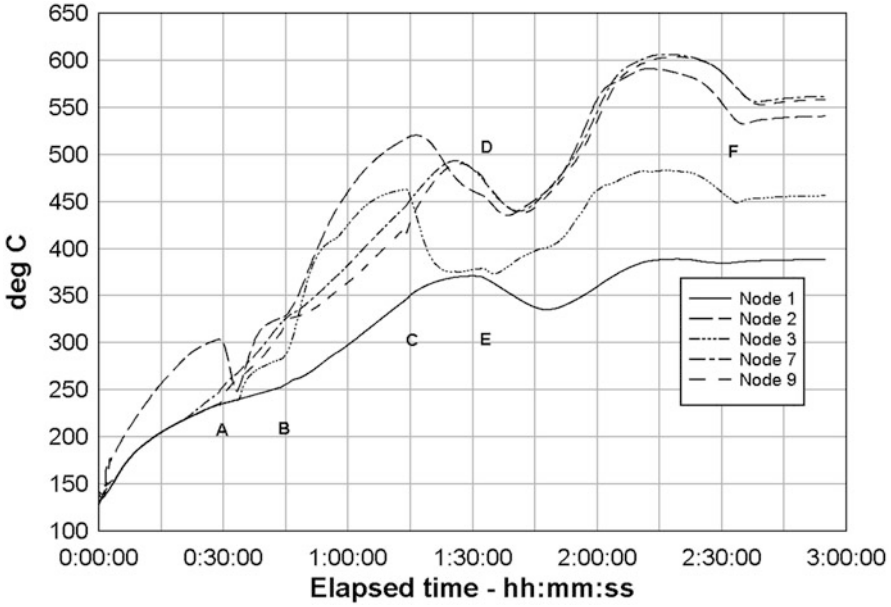

Fig. 17.4 Network temperature trends

The increase in steam specific enthalpy from drum to boiler outlet, assuming all the convective heat from the flue gas is transferred to the steam, will be 238,080 kJ/s / 330 kg/s or 721 kJ/kg. The specific enthalpy of steam at boiler outlet is then (2,493.8 + 721) or 3,215.3 kJ/kg. At the boiler outlet pressure of 16,700 kPa, this indicates a temperature of 477 °C, considerably less than the more typical 540 °C expected. The difference is made up by the radiant component which can be estimated as follows.

For the same pressure and 540°C, the steam enthalpy will be 3,382.1 kJ/kg or an increase of 166.8 kJ/kg. For the given steam flow of 330 kg/s, the radiant component to all radiant superheaters must add 55,044 kJ/s, say 55 MW. As we saw in Chap. 11, on the basis of some assumed distribution of radiant heat, around 35 MW might be transmitted to the secondary superheater in a boiler of similar dimensions and rating to the one in discussion here. It should be noted that the radiant component is transferred to the secondary and tertiary superheaters, which are the first elements in the flue gas path. The resulting higher tube temperatures will reduce the convective heat transfer to these superheaters and raise the gas temperatures seen further down the gas path, increasing the convective components of the later superheaters and reducing overall the requisite radiant components. These figures are therefore indicative only but they are consistent with those of the earlier chapter.

Since this is a discussion of the simulation method rather than of boiler design and operation, the numerical procedure itself is of primary interest. A good indicator

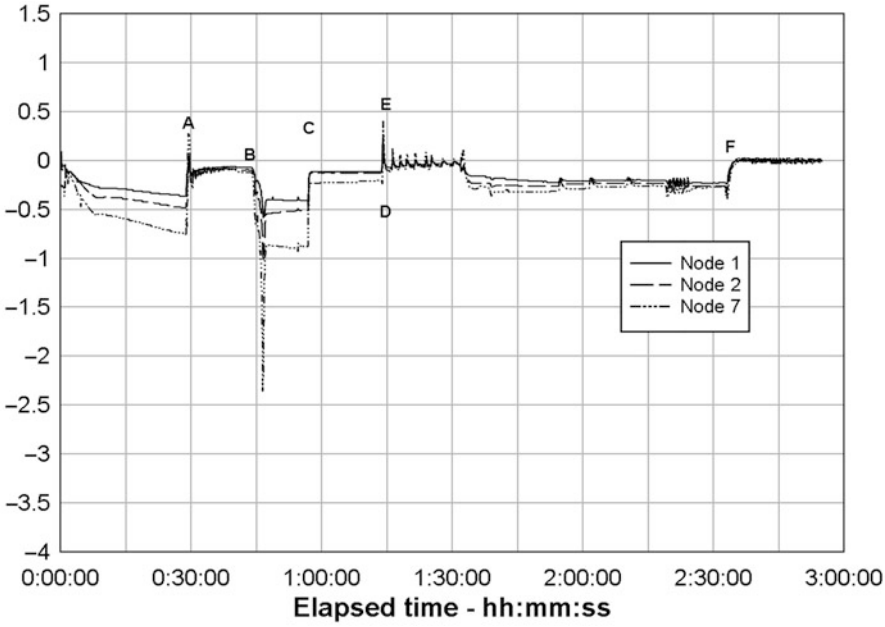

Fig. 17.5 Network node mass balance trends

of numerical performance is provided by the individual node mass balances. The formulation of the mass balance equation is intended to yield a steady-state solution showing zero mass balance for each node. Transient deviations from zero indicate adjustments to the node mass. Figure 17.5 shows the trends of the instantaneous node mass balances for selected nodes during these simulated operations. As can be seen, the node balances remain close to zero during transients and are practically zero during steady-state. Short-lived excursions away from zero accompany rapid changes in branch flows, such as at point B when the HP bypass valve closed.

The same operations were simulated using the augmented Eq. 17.46 with the same network parameters and node and branch tuning parameters. Visually, at the scale offered by these diagrams, no differences are observable. The node mass balance deviations produced by the fully integrated method were around half those produced by the unbundled method except in response to the rapid pressure loss (see below) for which both were almost identical. The network tuning parameters were chosen to give convergence of the iterative near-tridiagonal matrix solution within 30 iterations, though usually less than 10 sufficed to satisfy the convergence criteria. The unbundled method allowed up to five iterations but for most situations needed only one or two.

The numerical method was tested in an extreme case by the introduction of an unscheduled fault of unspecified nature that caused an extremely rapid loss of pressure to around 1,000 kPa and trip of the turbine. The salient features of this

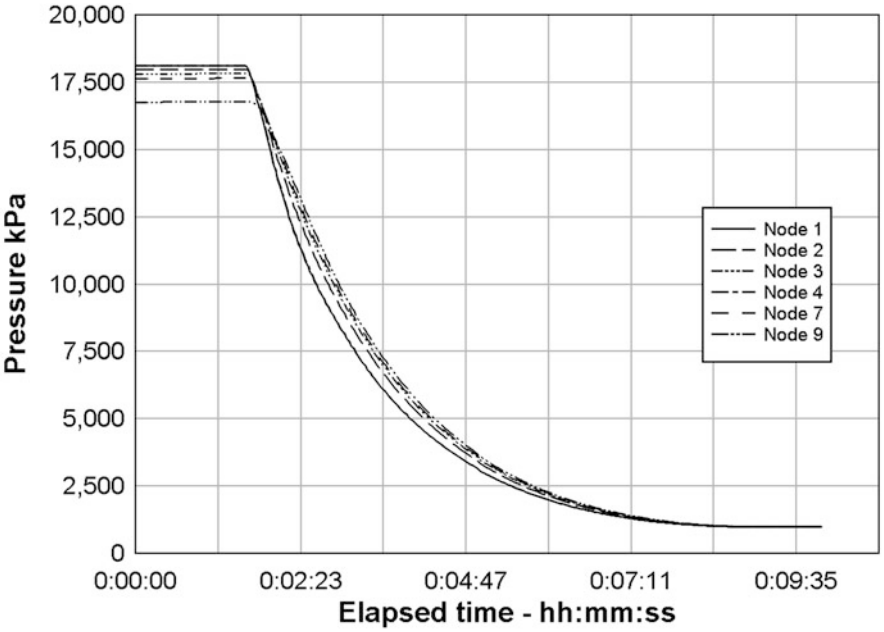

Fig. 17.6 Node pressure trends during an extreme pressure reduction

event are shown by Figs. 17.6 and 17.7. Turbine steam flows reduced to zero within a few seconds as the turbine valves shut. A pressure loss of this magnitude and speed might be expected only as a result of an extreme malfunction event, such as a steam pipe fracture, whose accurate reproduction is beyond this method. The event does however illustrate the dynamic response and numerical stability of the method, in even this extreme case.

Transiently, the node mass balances increased well beyond the values achieved when handling more normal rates of change, peaking at around 80 kg/s for node 3, though for a very short duration. The error at node 9, directly influenced by the rapid reduction of flow to the turbine, persisted for much longer.

The same extreme event was rerun using double the iteration count, and the results are shown by Figs. 17.8 and 17.9. The benefits of the higher iteration count are immediately apparent from the reduction in peak mass balance errors by around 30 % and the halving of their duration. However, the node mass balance deviations in this extreme case exceed those which might be expected given the physical node volumes and indicate the presence of significant dynamic errors. In the general case, increasing the iteration count will not be sufficient as the real-time constraint will limit the number of iterations to less than that required for convergence. Indeed, in the light of later comments, it must be expected that the solution will never converge, regardless of the number of iterations.

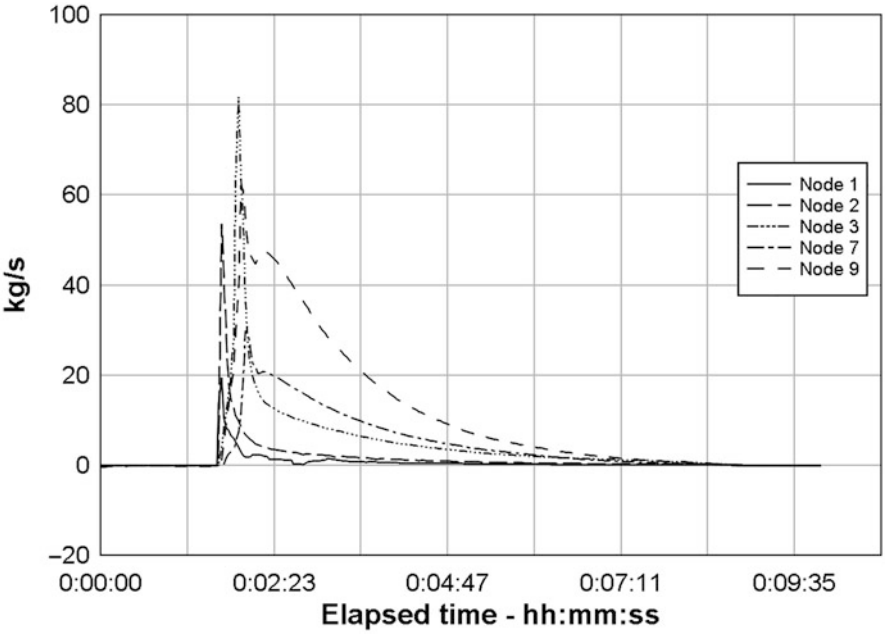

Fig. 17.7 Node mass balances during an extreme pressure reduction

Finally, a severe but operationally "normal" event is the opening of a boiler safety valve. Figures 17.10 and 17.11 show the responses of pressures and mass balances of the nodes closest to the SV attachment point to abrupt opening and subsequent closure of the boiler safety valve SV. Around 230 kg/s of steam flowed through the fully opened valve, being some 70 % of the boiler full-load capacity. The valve remained open for about 2 min before re-closing. Although by operational standards a major disturbance, this event is readily handled by the network computation. It should be noted that the illustrated behaviour is not that expected from the opening of a safety valve. For this simplified example, the boiler pressure is held constant, and the network solution shows the response to a sudden increase in steam flow which can be supplied by the boiler without loss of pressure. The reduction in pressure at the node connected to the valve is equal to the increased frictional pressure loss corresponding to the increased steam flow.

The inability of the method as described to yield node mass balances consistent with physical node volumes in extreme cases may be attributed to the neglect of flow momentum. Extremely rapid large pressure changes induce large and sudden forces on the working fluid masses which do not respond instantaneously, as assumed if momentum is ignored. Should dynamically accurate simulation of these extreme cases be the objective, the approach described above must be extended to include treatment of flow momentum. However, the illustrated numerical results suggest that, for all normal and even major but not extreme plant upsets, neglect of momentum will yield satisfactory results.

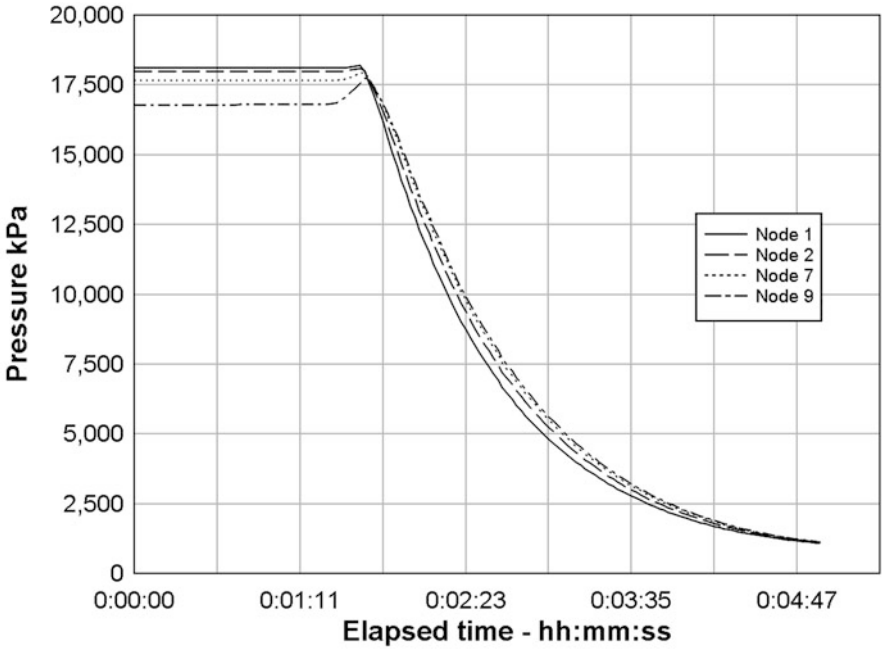

Fig. 17.8 Node pressures with increased iteration count

17.2.8 Inclusion of Flow Momentum

Equation 17.18 was derived for incompressible flow in a network branch. For compressible flow in a network cell, the same form applies but with the branch parameters ($\dot{m}_{ij}$, $\mathcal{A}_{ij}$ and I_M) replaced by their cell equivalents. Then

$$\dot{m}_j^{n+1} = \vartheta_j \, \dot{m}_j^n + \theta_j \, \Delta p_j^{n+1} \tag{17.50}$$

with

$$\theta_j = \frac{\Delta t \, \mathcal{A}_j}{I_M \, \mathcal{A}_j + 2\Delta t \, \dot{m}_j^n} \tag{17.51}$$

and

$$\vartheta_j = \frac{I_M \, \mathcal{A}_j + \Delta t \, \dot{m}_j^n}{I_M \, \mathcal{A}_j + 2\Delta t \, \dot{m}_j^n} \tag{17.52}$$

and an equivalent pair for the linearisation $\dot{m}^2 \approx \dot{m}^{n+1}\dot{m}^n$.

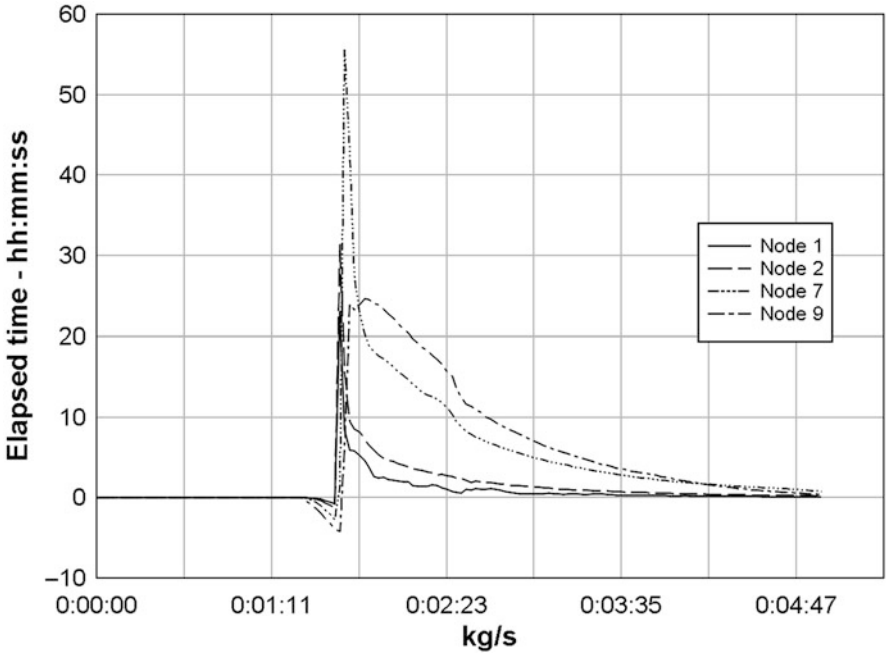

Fig. 17.9 Node mass balances with increased iteration count

Considering only the pressure equation from Eq. 17.28, and using Eq. 17.50 for $\dot{m}_{j-1}$ and $\dot{m}_j$, we arrive at the following equation for the pressure in the jth cell.

$$-a_1\frac{\Delta t}{|D|}\theta_{j-1}p_{j-1}^{n+1}+\left(1+a_1\frac{\Delta t}{|D|}(\theta_{j-1}+\theta_j)\right)p_j^{n+1}-a_2\frac{\Delta t}{|D|}\theta_j p_{j+1}^{n+1}$$
$$=p_j^n+a_1\frac{\Delta t}{|D|}\left(\vartheta_{j-1}\dot{m}_{j-1}^n-\vartheta_j\dot{m}_j^n\right). \tag{17.53}$$

Expanded for all cells in a branch this equation generates a tridiagonal matrix equation to be solved for all the cells in the branch, now including flow momentum. Boundary conditions are applied in the usual way.

The equation for the k-th node pressure including flow momentum is,

$$\left(1+\frac{\Delta}{\tau_k}\sum_j\theta_j\right)\bar{p}_k^{n+1}=\bar{p}_k^n+\frac{\Delta}{\tau_k}\left(\sum_j\vartheta_j\dot{m}_j^n+\sum_j\theta_j p_j^{n+1}+\sum\dot{m}_{ext}\right) \tag{17.54}$$

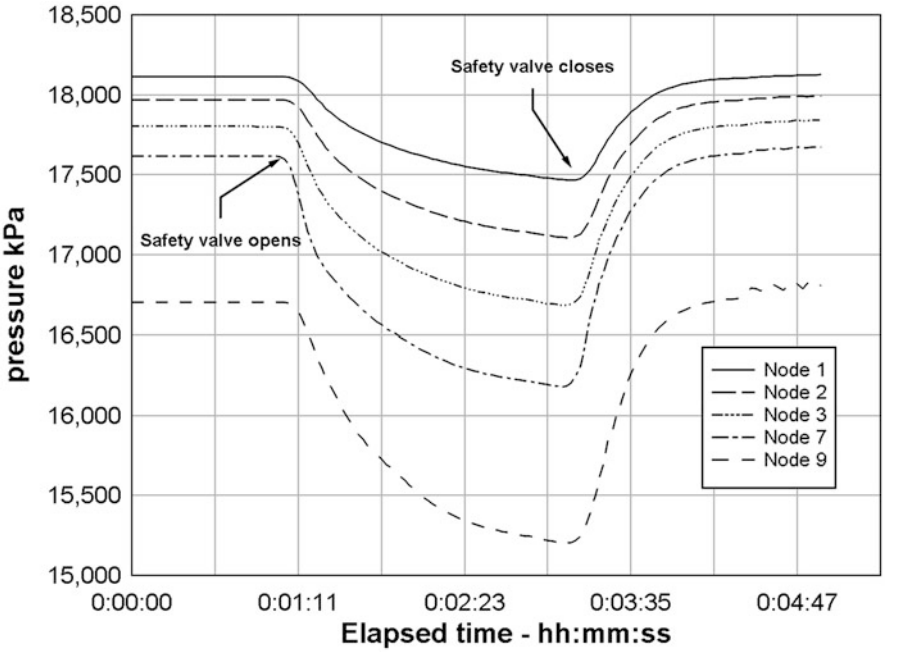

Fig. 17.10 Node pressure trends—operation of the SV

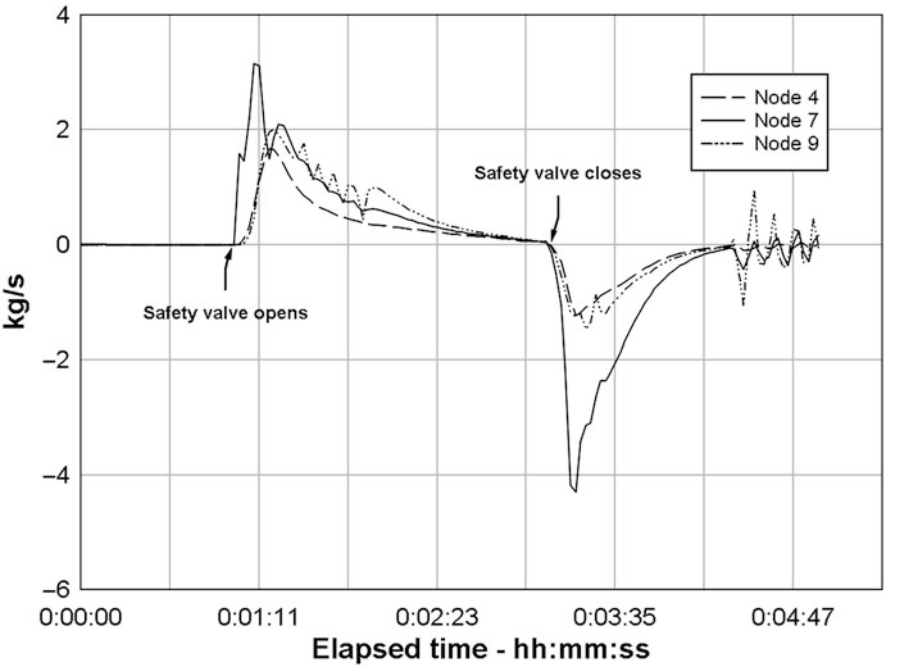

Fig. 17.11 Node mass balance trends—operation of the SV

Network Behaviour: Flow Momentum Included

The same network was subjected to the same start-up procedure, this time with flow momentum included. The results are shown by Figs. 17.12 and 17.13.

The variations of network pressures with momentum included are visually indistinguishable from those without momentum included[4]. The variations of node mass balances show differences of detail, but magnitudes remain small, within the same limits. These results allow the conclusion that, for these rates of change, flow momentum is not a significant factor.

The same however cannot be said of more rapid events. Figures 17.13 and 17.14 show the same results as Figs. 17.6 and 17.7, but now with momentum included. Most striking is the reduction of the magnitude of the node mass balances from around 80 kg/s with a tail >2 kg/s persisting for several minutes, to a sharp peak of less than 2.5 kg/s and a tail of <0.5 kg/s. The duration of the transient, being the time to achieve steady state, increased from around 7 to around 15 min as the effect of momentum caused things to change more slowly. These results allow the conclusion that large rapid transient events cannot be accurately reproduced or predicted if flow momentum is ignored.

It is interesting to note that inclusion of flow momentum adds very little to the computation load. The dimensions and population of the describing coefficient matrices are the same with or without momentum, there being only the minor addition of computation of the ϑ and θ terms (Fig. 17.15).

[4]The slightly closer spacing of the individual traces in Fig. 17.12 is the result of the use of somewhat larger pipes in this case.

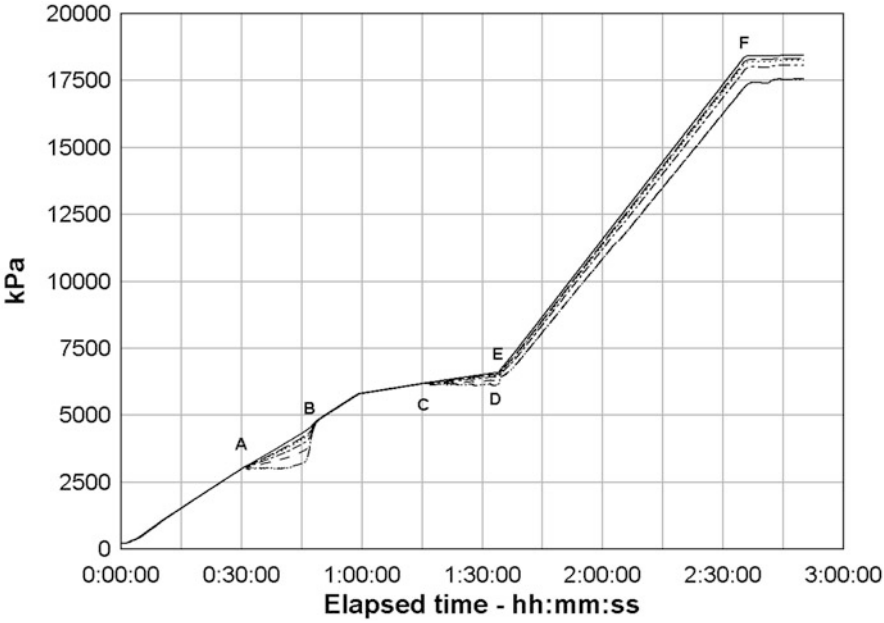

Fig. 17.12 Network pressures during start, including flow momentum

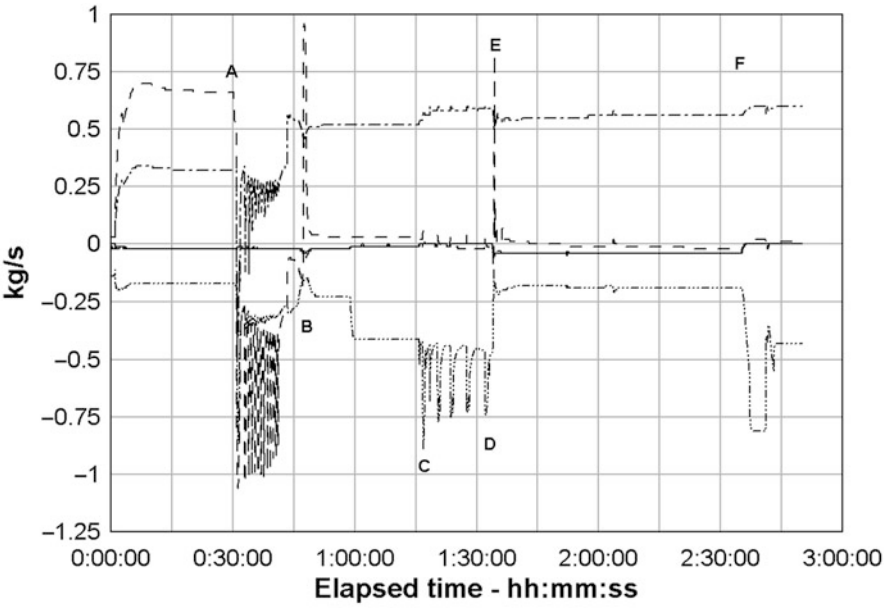

Fig. 17.13 Network node balances during start, including flow momentum

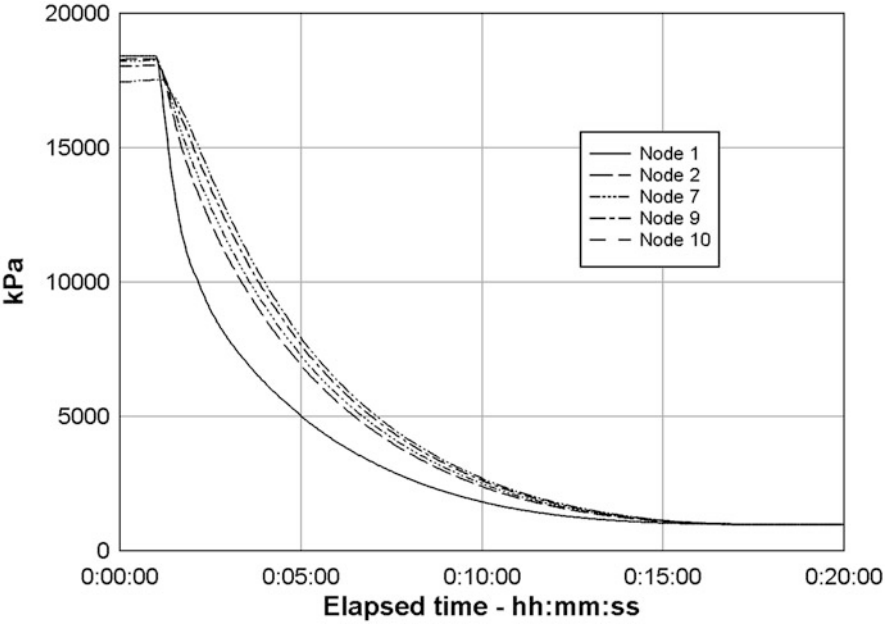

Fig. 17.14 Network pressures during rapid depressurisation

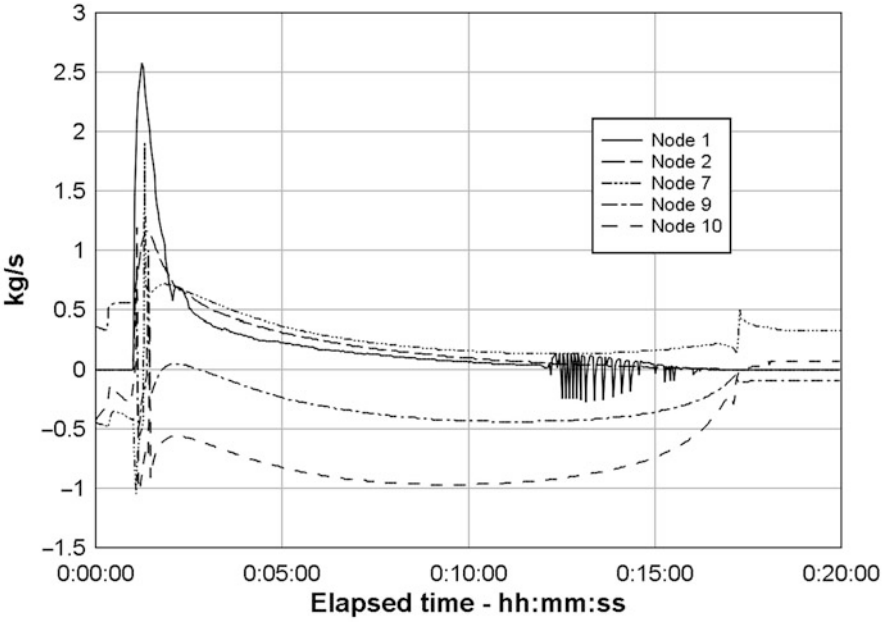

Fig. 17.15 Node balances during rapid depressurisation